Modern Physics Letters B
Vol. 34, No. 25 (2020) 2050269 (12 pages)

DOI: 10.1142/S0217984920502693

Effect of rolling deformation on microstructure and mechanical properties of 2205 duplex stainless steel with micro-nano structure

Yuqi Mao[*,§], Yuehong Zheng[*,¶], Yu Shi[*,‖], Min Zhu[*,**], Saitejin[†,††], Sen Liu[‡,‡‡], Xiaoliang Lin[‡,§§] and Peiqing La[*,¶¶]

[*]*State Key Laboratory of Advanced Processing and Recycling of Nonferrous Metals, Lanzhou University of Technology, Lanzhou 730050, China*
[†]*Institute of Stainless Steel Research, Iron and Steel Institute, Jiuquan Iron and Steel Corporation, Jiayuguan 735100, China*
[‡]*Technology Center Central Laboratory, Jiuquan Iron and Steel Corporation, Jiayuguan 735100, China*
[§]*maoyuqi1214@163.com*
[¶]*zhengyuehong1986@126.com*
[‖]*32227014@qq.com*
[**]*zhumin@lut.edu.cn*
[††]*jinsaite@jiugang.com*
[‡‡]*liusen@jiugang.com*
[§§]*linxiaoliang@jiugang.com*
[¶¶]*pqla@lut.edu.cn*

Received 19 January 2020
Revised 24 February 2020
Accepted 27 February 2020
Published 1 July 2020

In order to further expand the application scope of 2205 duplex stainless steel (DSS), its microstructure and mechanical properties require as much attention as its corrosion properties. In this study, 2205DSSs were prepared by aluminothermic reaction and the microstructures and mechanical behavior of the rolled alloys were analyzed. The micro-nanocrystals composite structure appears in the alloys after rough rolling with deformation of 40% at 1000°C followed by finishing rolling with deformation of 30%, 50% and 70% at 600°C. With the increase of rolling deformation, the two-phase structure is gradually elongated, the average size of the two-phase grains is gradually increased, and some γ phase will change to α phase, the volume fraction of α phase is gradually increased, and the distribution of nanocrystals is gradually uniform. Meanwhile, the fracture mode of alloy is gradually changed from ductile fracture to brittle fracture. The strength and hardness of the alloy increase gradually.

Keywords: 2205 Duplex stainless steel; rolling; microstructure; mechanical property; aluminothermic reaction.

[¶¶]Corresponding author.

1. Introduction

2205 Duplex stainless steel (DSS) is composed of ferrite (α) and austenite (γ) phases (the less phase accounts for at least 30%[1–4]), which combines the advantages of these two phases and has good mechanical properties and chloride stress corrosion resistance. It is widely used in shipbuilding, petrochemical industry, oil and gas pipeline, paper industry, deep sea pipeline and other fields.[5–10]

For 2205 DSS, researchers have paid more attention to its corrosion resistance and the corrosion resistance of welded joints.[11–14] But as a kind of engineering steel, its mechanical properties such as toughness and strength also need to be concerned, which can further expand its application scope and prolong its service life. Traditionally, grain refinement is one of the main ways to improve the strength of steels. However, grains reach the nanometer level, and the strength can be greatly improved, but there is almost no local strain due to lack of work hardening in the process of deformation at room temperature.[3–5] Aiming at the common problem of high strength and low plasticity in nanocrystalline steel, the micron-scale grains are introduced into the nanocrystalline matrix to form a novel micron/nanocrystalline composite structure, which plays the role of balancing strength and ductility.[15]

At present, powder metallurgy and large plastic deformation are the main methods to prepare microcomposite/nanocomposite structural alloys. The powder metallurgy process[16,17] is to mix, compact and sinter microncrystal and nanocrystal powders to form composite structure. Although the method can regulate the proportion of microcrystal and nanocrystal in the bimodal structure, it is easy to produce pores in the processing process that cannot be eliminated by annealing, thus affecting the material performance. In addition, the cost of this method is relatively high.[18] Compared with powder metallurgy process, large plastic deformation can produce denser and cleaner materials, mainly in the form of equal channel angular pressing (ECAP) and high-pressure torsion (HPT). For ECAP,[19,20] the ultrafine/nanocrystalline was obtained first and then annealed to make some of the ultrafine grains recrystallize and grow up, so as to obtain the heterogeneous structure of the micron grains embedded in the ultrafine/nanocrystalline matrix, but it is difficult to control the ideal bimodal structure by annealing. Different from ECAP, the specimen prepared by HPT can obtain a more uniform microstructure. However, this method can only process relatively thin samples and is largely limited by equipment and mold. Therefore, it is difficult to get practical application in industry.

In view of the limitations of the above methods in the production of large-scale samples, our group focused on the preparation of microstructure/nanostructure alloy by aluminothermic reaction. The method is to accurately weigh Fe_2O_3 powder and Al powder according to the stoichiometric ratio of aluminothermic reaction formula and add other required alloy powder to reach the chemical composition of the required steel. The aluminothermic reaction between iron oxide and aluminum powders is carried out under the protection of argon and initiated by the reaction

of ignition agent at a lower temperature (260°C). Then a large amount of heat is generated and it can reach the temperature to 2727°C, which is about 927°C higher than the melting point of reaction product and by-product alumina. Thus, the large superheat degree can make the solution of alloy and alumina overheated and purified.[21] With the decrease of temperature, a small amount of grains first nucleate in the molten steel and gradually grow into micron crystals. When the temperature is reduced to the effective nucleation temperature, the nucleation rate increased sharply. Moreover, a large degree of supercooling and a high cooling rate (about 150 K/s) appear in the molten steel due to the high thermal conductivity of the copper substrate, which makes the grains in the remaining liquid stainless steel nucleate quickly but grow up slowly; therefore, most of these grains are nanocrystals after solidification. Thus, the microstructure/nanostructure can be directly prepared by aluminothermic method.[22–24] It can be seen that the aluminothermic reaction method not only has the advantages of low energy consumption, low cost and simple process, but also has the potential of industrial production because it can obtain large-scale ingots.

In our previous work,[21,25,26] the large-scale nanocrystalline Fe–Al–Cr alloy, microstructure/nanostructure 316L and 304 austenitic stainless steels have been successfully prepared by aluminothermic reaction method, and their heat treatment structures and mechanical properties have been studied. Therefore, in this paper, 2205 DSS will be prepared by aluminothermic reaction and the effect of rolling with different deformations on the microstructure and mechanical properties will be analyzed. Furthermore, the fracture mechanism of the alloy with different deformations will be discussed in detail.

2. Experiments

In this paper, 2205 DSS samples were prepared by aluminothermic reaction. The chemical composition of the 2205 DSS is Cr: 21.8, Ni: 5.36, Mo: 2.68, Si: 0.74, Mn: 0.75, Al: 1.18 (wt.%) and Fe balance. First, the proportion of main reactants was calculated accurately according to the chemical reaction formula (1), and the proportion of other alloy elements was determined according to the composition range of each element in 2205 DSS. Second, the reaction powders are weighed, mixed and put into the stainless steel ball grinding tank of QM-1SP4 planetary ball mill to mill for 8 h at the speed of 150 r/min. Third, the powers pressed into several billets with the size of Φ 85 mm $\times$ 15 mm. The billets were placed in the copper crucible and 3 g of flaky igniting agent was put at the top of billets. Finally, Cu crucible was put in the reaction vessel, and 0.5 MPa argon was filled in the closed reaction vessel to exhaust the air at room temperature. When the temperature of the raised to 200°C, the remaining argon was discharged again to release water vapor and residual air. Then, the autoclave was refilled with 4 MPa argon and increases the temperature. As the temperature reached about 260°C, the ignition agent started to react and released a large amount of heat, which caused

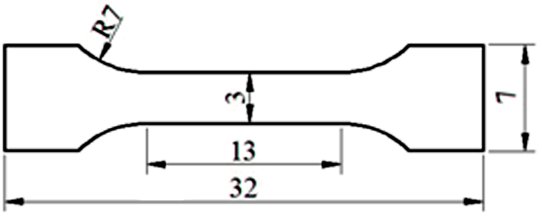

Fig. 1. Schematic diagram of tensile sample (mm).

the reaction between the reaction materials. After the reaction, samples were cooled to room temperature with the furnace:

$$Fe_2O_3 + 2Al = 2Fe + Al_2O_3. \quad (1)$$

The as-cast samples were cut into $100 \times 50 \times 5$ mm^3 cubes by wire cutting. In order to eliminate the casting defects and improve the ductility of the steel, the alloy was rolled roughly with deformation of 40% at 1000°C and then rolled fine with deformation of 30%, 50% and 70% at 600°C. All samples were cooled to room temperature in the air after rolling.

AJSM-6700F scanning electron microscope (SEM) was used to analyze the microstructure, and a D/Max-2400 X-ray diffractometer (XRD) and a JEM2010 transmission electron microscope (TEM) operating at 200 kV were used to characterize the structure of the samples. The TEM samples were thinned electrolytically with a twin-jet electro-polishing device in a solution of 2 vol.% perchloric acid in ethanol. AHXD-2000TMSC/LCD microhardness tester was used for hardness test. The AGS-X universal mechanical testing machine is used to conduct the tensile test at the cross speed of 0.2 mm/min, and the average value is repeated three times, with the standard deviation less than 5%. The size of the tensile sample is shown in Fig. 1.

3. Results

Figure 2 shows the XRD patterns of 2205 DSSs with rolling deformation of 30%, 50% and 70% at 600°C. With the increase of rolling deformation, the intensity of the diffraction peak of γ phase decreases and that of α phase increases. The average grain size of the two phases can be calculated by Scheler's formula. The formula is given as follows:

$$D = K\lambda/B\cos\theta, \quad (2)$$

where d is the average grain size, K is constant 0.9, λ is the characteristic X-ray wavelength, B is the full width at half maximum and θ is the diffraction angle. The results show that the grain size of α phase with 30%, 50% and 70% deformation at 600°C is 30, 34 and 52 nm, respectively, and that of γ phase is 48, 57 and 72 nm, respectively. Namely, the average grain size increases with the increase of rolling deformation.

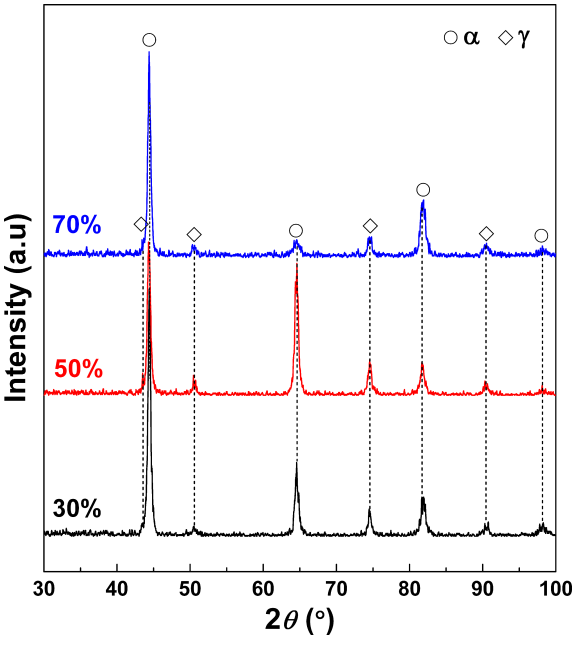

Fig. 2. XRD patterns of 2205 DSSs with rolling deformation of 30%, 50% and 70% at 600°C.

Figure 3 shows the SEM images of 2205 DSSs with rolling deformation of 30%, 50% and 70% at 600°C. The phase boundaries of the α and γ phases can be clearly seen from the figure. The phase boundaries are gradually elongated with rolling deformation from 30% to 70%, and there is uneven rolling on the rolled alloys. The volume fractions of α and γ phases in 10 photos selected from the rolled 2205 DSSs were counted by ipwin6 software and the average values were obtained. The volume fractions of α in the alloys with rolling deformation of 30%, 50% and 70% were 58%, 62% and 69%, respectively. It can be seen that the volume fraction of α increased with the increase of rolling deformation, which is consistent with the results of XRD that the intensity of the diffraction peaks of the α phase increases with the increase of rolling deformation.

Figures 4 and 5 show the TEM analysis results of 2205 DSSs with deformation of 50% and 70% at 600°C, respectively. Figures 4(a) and 4(b) and 5(a) and 5(b) show bright field images and dark field images of a certain region of two samples. There are black, gray and white regions in the bright field images, which are microcrystal (>1 μm), submicrocrystal (100–1000 nm) and nanocrystal (<100 nm). The bright white spots in the dark field are nanocrystallines, which can diffract electron beam strongly because of its relatively small grain size and random orientation. Therefore, the corresponding selected area electron diffraction (SAED) patterns (Figs. 4(c) and 5(c)) also show the continue diffraction rings. The diffraction rings have bright spots, which indicates that the preferred orientation of the steel is produced in the rolling

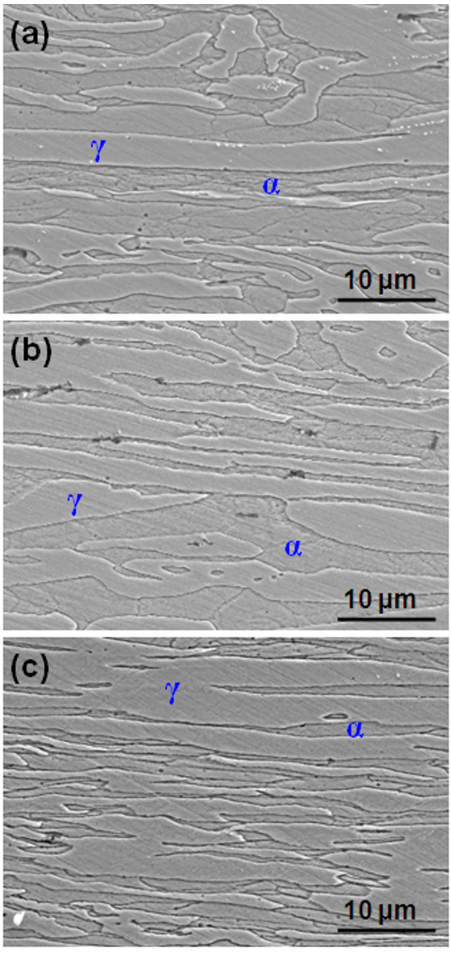

Fig. 3. SEM images of 2205 DSSs with rolling deformation of (a) 30%, (b) 50% and (c) 70% at 600°C.

process. The calibration of the diffraction ring shows that the nanocrystals are mainly the γ phase (face-centered cubic structure) and the α phase (body-centered cubic structure). In addition, a small amount of Al_2O_3 nanocrystals were also observed in the alloys.

Figure 6 shows the histograms of grain size distribution of the nanocrystalline of 2205 DSSs with rolling deformation of 50% and 70% at 600°C. It is visible that the grain size of nanocrystalline ranges from 10 to 60 nm and from 20 to 80 nm, corresponding to the deformation of 50% (Fig. 6(a)) and 70% (Fig. 6(b)), respectively. By comparison, when the rolling deformation is 70%, the average size of nanocrystalline tends to increase, but the grain distribution is better.

Figure 7 shows the stress–strain curves of 2205 DSSs with different rolling deformations at 600°C. The relevant mechanical property parameters are listed

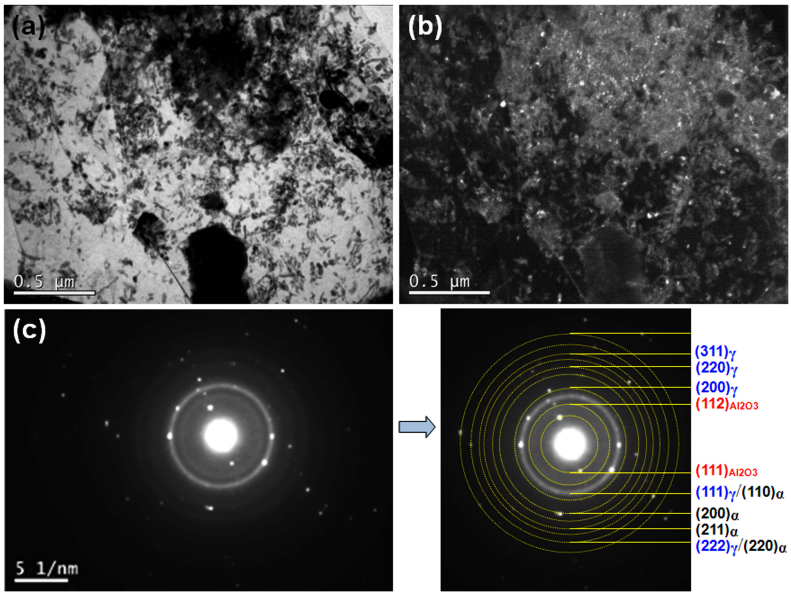

Fig. 4. TEM images of the microcrystalline/nanocrystalline structured 2205 DSS with rolling deformation of 50% at 600°C: (a) bright field image, (b) dark field image and (c) the corresponding SAED pattern.

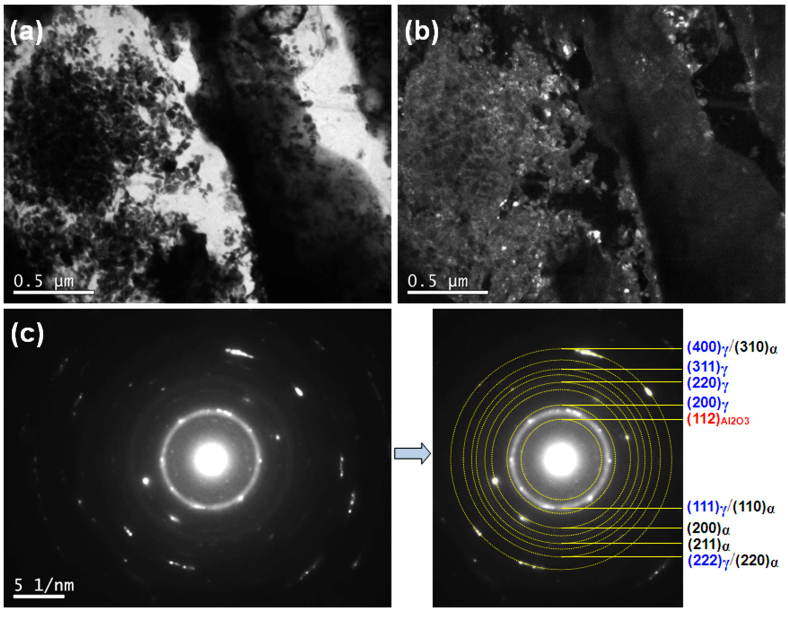

Fig. 5. TEM images of the microcrystalline/nanocrystalline structured 2205 DSSs with rolling deformation of 70% at 600°C: (a) bright field image, (b) dark field image and (c) the corresponding SAED pattern.

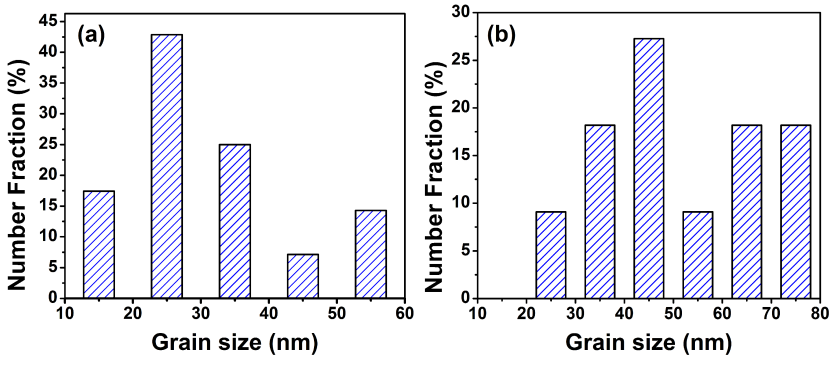

Fig. 6. Histograms of grain size distribution of the nanocrystalline of 2205 DSSs with rolling deformation of 50% (a) and 70% (b) at 600°C.

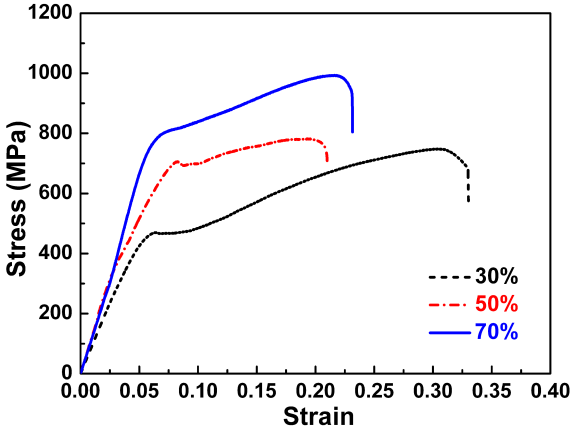

Fig. 7. (Color online) Stress–strain curves of 2205 DSSs with rolling deformation of 30%, 50% and 70% at 600°C.

Table 1. Mechanical property parameters of 2205 DSSs with different rolling deformations.

Rolling deformation (%)	$\sigma_{0.2}$ (MPa)	σ_b (MPa)	δ (%)	Hardness (HV)
30	470	745	32.5	328.44
50	703	781	23.0	338.70
70	796	998	24.8	355.30

in Table 1. For the alloys with rolling deformation of 30%, 50% and 70%, the tensile strength (σ_b) is 745, 781 and 998 MPa, the yield strength ($\sigma_{0.2}$) is 470, 703 and 796 MPa, the elongation (δ) is 32.5%, 23% and 24.8%, the hardness is 328.44, 338.70 and 355.30 HV, respectively. Namely, the strength and hardness increase with the increase of rolling deformation at the same rolling temperature.

However, according to the empirical conversion formula of hardness and strength, which is as follows[27]:

$$\sigma_b = 9.8 \times \left(\frac{2463622}{3031 - \mathrm{HV}} - 801.633 \right). \tag{3}$$

The tensile strength of 2205 DSSs with rolling deformation of 30%, 50% and 70% can be calculated as 1078, 1112 and 1167 MPa, respectively. That is, there is a certain difference between the actual measured values of tensile strength and the calculated values. The main reason is that the fracture section needs to be further analyzed.

Figure 8 shows the low-magnification and high-magnification fracture morphologies of 2205 DSSs with rolling deformation of 30%, 50% and 70% at 600°C. It can be seen from Figs. 8(a) and 8(b) that there are a large number of deep and

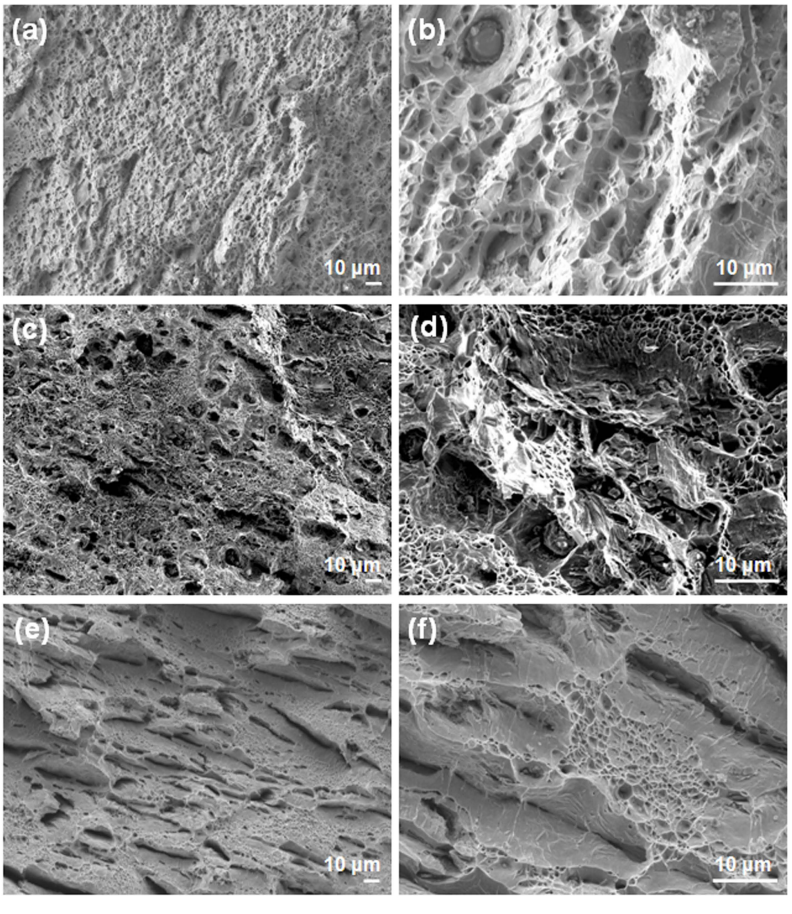

Fig. 8. Low-multiple and high-multiple fracture morphologies of 2205 DSSs with different rolling deformations: (a, b) 30%, (c, d) 50% and (e, f) 70%.

dense dimples on the fracture surface when the rolling deformation is 30%, which shows that the tensile stress is evenly distributed on the fracture surface, and the microcavities grow uniformly in three directions to form the equiaxed dimples. The fracture mode is ductile fracture, showing a good plastic shape. When the deformation increases to 50% (Figs. 8(c) and 8(d)), there are still a large number of dimples on the fracture surface, but compared with the sample of 30% deformation, the dimples are relatively small and shallow, and a small amount of cleavage surface appears. The fracture mode is mixed of ductile and brittle. In addition, Al_2O_3 inclusions are found in some dimples of the fracture surface of the sample. These inclusions and the second phase particles play an important role in the fracture of the dimples. Because the inclusions will cause the particle and the matrix not to bond firmly, easy to crack, generate micropores and easy to fracture under the continuous action of tensile force. Therefore, when the deformation is 50%, although its strength is next to that of the sample with 30% deformation, it is easy to fracture and its elongation is the lowest. When the rolling deformation is 70% (Figs. 8(e) and 8(f)), the fracture surface is mainly a large number of cleavage surfaces, only a small number of small and shallow dimples, showing the typical morphology of brittle fracture.

4. Discussion

When the rolling deformation of 2205 DSS increases at 600°C, the transformation from γ phase to α phase occurs. The first reason is that when the DSS is hot worked in the range of 500–1600°C, the crystal defect density of γ phase will increase, resulting in the increase of nucleation particles of α phase.[28] Second, deformation makes the shape of γ phase grain change and the area of grain boundary in unit volume increases. The grain boundary of γ and the interface of γ/α can be used as the nucleation point of α phase,[29,30] that is, the position of α phase nucleation increases. Third, with the increase of rolling deformation, there are a lot of dislocation plug in grain boundary and crystal, and the internal stress of alloy will increase accordingly, so as to guide the driving force of phase transformation is enhanced, which further promotes the transformation from γ to α phase.[29,30] Therefore, with the increase of deformation, the volume fraction of α phase increases, while that of γ phase decreases. On the other hand, the grain growth tendency of 2205 DSS is higher than the degree of crushing, and the grain size increases with the increase of rolling deformation.

It is precisely because the volume fraction of α and γ phases and the grain size will change with increasing rolling deformation. Therefore, the mechanical behavior of the alloys will be different under different rolling deformations. In the process of tensile deformation, the relatively soft γ phase in the early stage of deformation will accommodate most of the plastic deformation. When the γ phase cannot continue to bear the deformation, the relatively hard α phase has poor toughness which leads the alloy fracture soon. Therefore, when the volume fraction of γ phase is

high, the toughness of steel is relatively good but the strength is relatively poor. On the contrary, when the volume fraction of α phase is high, the strength is good and the hardness is high, but the toughness is poor.

However, it should be noted that the two-phase grain size increases with the increase of deformation, that is, the strength and grain size of the alloy do not meet the Hall–Petch relationship. For nanocrystalline strength, Luke *et al.*[31–33] found that the strength does not always increase infinitely with the decrease of grain size. When the grain size is small to nanoscale, it is difficult to hold dislocations in the grain, which leads to the transformation of the plastic deformation mechanism from dislocation sliding to grain boundary sliding, namely, the classical Hall–Petch relationship is no longer applicable. But here, the average grain size is above 30 nm, which is not small enough to invalidate the Hall–Petch relationship. Therefore, it is indeed inappropriate to discuss such an inverse Hall–Petch relationship. For 2205 DSS with microstructure/nanostructure, when the rolled steel is under tensile deformation, the hard nanocrystalline phase bears most of the tensile load, while the soft nanocrystalline phase only bears a small part of the stress. Thus, the uniform distribution of nanoparticles can avoid the stress concentration and make the nanocrystals and microncrystals bear the stress to the maximum extent, which will improve the strength. In addition, the uniform distribution of nanoparticles can effectively pin dislocations and grain boundaries, which can enhance the driving force of dislocation movement and then improve the yield strength and hardness. According to the statistical results of nanocrystalline size, the nanocrystalline distribution of the alloy with large deformation is better. Therefore, the strength and hardness increase with the increase of rolling deformation.

5. Conclusions

In this study, 2205 DSS with microstructure–nanostructure was prepared by aluminothermic reaction method and then was roughly rolled with deformation of 40% at 1000°C followed by finishing rolling with deformation of 30%, 50% and 70% at 600°C. The mechanism of deformation structure and mechanical behavior was discussed in detail. The results show that the micro-nanocrystals composite structure appears in the alloys after finishing rolling. With the increase of rolling deformation, the two phases are gradually elongated, the average grain size of the two-phase is gradually increased, and some γ phase will change to α phase, the volume fraction of α phase is gradually increased. For mechanical properties, the fracture mode of alloy is gradually changed from ductile fracture to brittle fracture when the rolling deformation increases from 30% to 70%. Meanwhile, the strength and hardness increase gradually. When the rolling deformation is 30%, 50% and 70%, the corresponding tensile strength is 745, 781 and 998 MPa, the yield strength is 470, 703 and 796 MPa, the elongation is 32.5%, 23% and 24.8%, and the hardness is 328.44, 338.70 and 355.30 HV, respectively.

Acknowledgment

This work is supported by the National Natural Science Foundation of China (Grant No. 51561020).

References

1. H. Liu *et al.*, *J. Wuhan Univ. Tech.* **30** (2015) 591.
2. I. Calliar *et al.*, *J. Mater. Sci.* **46** (2011) 6916.
3. M. Breda *et al.*, *Metall. Mater. Trans. A* **46** (2014) 577.
4. M. A. García-Rentería *et al.*, *Appl. Surf. Sci.* **321** (2014) 252.
5. O. J. Gerald *et al.*, *Mater. Chem. Phys.* **239** (2020) 122010.
6. P. D. Chen *et al.*, *Phys. Test.* **30** (2012) 11.
7. V. Stergiou and G. D. Papadimitriou, *J. Mater. Sci.* **47** (2011) 2110.
8. J. Yan *et al.*, *Metall. Mater. Trans. B* **46** (2015) 1461.
9. S. K. Ghosh *et al.*, *Bull. Mater. Sci.* **35** (2011) 839.
10. J. Yan, *et al.*, *J. Mater. Eng. Perform.* **23** (2014) 1157.
11. M. M. Sharma and C. Ziemian, *J. Mater. Eng. Perform.* **17** (2008) 870.
12. V. S. Sinyavskii, *Prot. Met.* **37** (2001) 469.
13. H. Y. Liou, R. I. Hsieh and W. T. Tsai, *Corros. Sci.* **44** (2002) 2841.
14. S. Geng *et al.*, *J. Manuf. Processes.* **19** (2015) 32.
15. W. Yinmin *et al.*, *Nature.* **419** (2002) 912.
16. J. Beck *et al.*, *J. Electron. Mater.* **41** (2012) 1595.
17. Y. Liu *et al.*, *Jom.* **68** (2016) 899.
18. G. Wegmann, R. Gerling and F. P. Schimansky, *Acta Mater.* **51** (2003) 741.
19. H. W. Höppel *et al.*, *J. Phys.* **240** (2010) 012147.
20. S. Zherebtsov *et al.*, *Mater. Sci. Eng. A* **536** (2012) 190.
21. P. Q. La *et al.*, *Metall. Mater. Trans. A* **45** (2014) 5236.
22. P. La *et al.*, *Mater. Sci. Eng. A* **561** (2013) 317.
23. P. La *et al.*, *Adv. Mater.* **18** (2006) 733.
24. P. La *et al.*, *Mater. Sci. Eng. A* **527** (2010) 2313.
25. P. Q. La *et al.*, *Int. J. Self Propag. High Temp. Synth.* **21** (2012) 89.
26. P. La, *et al.*, *Philos. Mag. Lett.* **94** (2014) 478.
27. Q. S. Wang, *Phys. Test. Chem. Analy.* **31** (1995) 39.
28. J. Calvo *et al.*, *Mater. Sci. Eng. A* **520** (2009) 90.
29. R. Bengochea, B. López and I. Gutiérrez, *Mater. Sci. Forum.* **284** (1998) 201.
30. F. Czerwinski *et al.*, *J. Mater. Sci.* **34** (1999) 4727.
31. K. Lu, X. D. Liu and Z. Q. Hu, *J. Mater. Res.* **8** (1994) 385.
32. C. S. Pande and K. P. Cooper, *Prog. Mater. Sci.* **54** (2009) 689.
33. T. G. Desai, P. Millett and D. Wolf, *Mater. Sci. Eng. A* **493** (2008) 41.